Supporting Information

Carrier Step-by-step Transport initiated by precise defect distribution engineering for Efficient Photocatalytic Hydrogen Generation

Jiewei Chen[1], Gaoxiang Wu[1], Tianyue Wang[1], Xiaodan Li[1], Meicheng Li[1,2]*,

Yuanhua Sang[3], Hong Liu[3]

[1]*State Key Laboratory of Alternate Electrical Power System with Renewable Energy Sources, North China Electric Power University, Beijing, 102206, China*

[2]*Chongqing Materials Research Institute, Chongqing 400707, China*

3 State Key Laboratory of Crystal Materials, Shandong University, Jinan 250100, China

* Corresponding author information: E-mail: mcli@ncepu.edu.cn; Fax: +86 10 6177 2951; Tel: +86 10 6177 2951.

1. Reaction mechanism of synthesizing designed TiO_2

To tailor the defect distribution in the defective TiO_2 for our design, it's necessary to clarify the reaction mechanism and control the forming process of the defective TiO_2. Here, we have precisely investigated the effects of surfactant HF on the properties of the prepared defective TiO_2, so as to understand the reaction mechanism in the hydrolysis process. To identify different prepared samples, hereafter we marked the sample as '$R_{F\text{-}X}$' (F means the surfactant is HF, and X is the raw material mole ratio of F:Ti).

Figure S1a shows the XRD patterns of our prepared samples $R_{F\text{-}0}$, $R_{F\text{-}2}$, $R_{F\text{-}4}$ and $R_{F\text{-}6}$. For $R_{F\text{-}0}$, a broad peak at 2θ = 25.3° corresponding to the (1 0 1) plane diffraction of anatase TiO_2 (JCPDS No. 21-1272) is observed. The broadening of the diffraction peak is caused by weak crystallization of the sample. With the increasing relative mole ratio of F:Ti from 0 to 6, the peak intensities of anatase increase, indicating an enhancement of crystallization because fluoride can enhance the crystallinity of anatase. It was reported that the presence of fluoride ions at low pH can accelerate the crystallization and growth of TiO_2 because of the rapid in situ dissolution–recrystallization, which reduces the concentration of defects in the TiO_2 lattice (Eqs. (1) and (2))[1] and enhances the formation of the well-crystallized TiO_2 crystals.

$$4H^+ + TiO_2 + 6F^- \rightarrow TiF_6^{2-} + 2H_2O \text{ (Dissolution)} \quad (1)$$

$$TiF_6^{2-} + 2H_2O \rightarrow 4H^+ + TiO_2 + 6F^- \text{ (Recrystallization)} \quad (2)$$

However, with the relative mole ratio of F:Ti increasing from 4 to 6, an obvious peak appears at 2θ = 23.4°, corresponding to the (1 0 0) plane diffraction of $TiOF_2$ (JCPDS No. 01-0490). This result reveals $TiOF_2$ can be formed under the high concentrated HF solution which may strongly affect the hydrolysis process. What's more, the SEM images of the samples (Figure S2) show that $R_{F\text{-}0}$ is the sphere-like shape varying from 300 nm to 3 μm, while $R_{F\text{-}2}$, $R_{F\text{-}4}$ and $R_{F\text{-}6}$ are nanosheet-like about 25 nm, well corresponding to the XRD spectra (Figure S1a).

The high resolution XPS F1s spectra of $R_{F\text{-}0}$, $R_{F\text{-}2}$, $R_{F\text{-}4}$ and $R_{F\text{-}6}$ (Figure S1b) show that there exist both physically adsorbed F (the peak at 684.4 eV) and lattice substituted F (the peak at 689.0 eV) in the $R_{F\text{-}2}$, $R_{F\text{-}4}$ and $R_{F\text{-}6}$. The intensity of the lattice substituted F increases as the mole ratio of F:Ti increases from 0 to 4, but decreases from 4 to 6, indicating that the appearance of $TiOF_2$ hinders the lattice substitution by F in the reaction process. Figure S1c shows the EPR patterns of our prepared samples with different relative ratios of F:Ti. For $R_{F\text{-}0}$, there only exists Ti^{3+}_{surf} . When the relative ratio of F to Ti increases to 2, there exist both Ti^{3+}_{surf} and $Ti^{3+}_{sub-surf}$. When the relative ratio of F to Ti increases from 2 to 4, the relative concentration of Ti^{3+}_{surf} keeps stable while the concentration of $Ti^{3+}_{sub-surf}$ increases. However, when the relative ratio of F to Ti increases from 4 to 6, the concentration of $Ti^{3+}_{sub-surf}$ decreases. Thus, the variation trend of the $Ti^{3+}_{sub-surf}$ is consistent with that of lattice substituted F as the relative ratio of F to Ti increases from 0 to 6. Since the $Ti^{3+}_{sub-surf}$ are closely related to the lattice substituted F, it's proposed that $Ti^{3+}_{sub-surf}$ comes from the substitutional doping of F into the TiO_2 lattice, because each fluorine atom that substitutes for an oxygen atom

can contribute an electron to the conduction band, which leads to the unpaired electron,[2] producing EPR signatures for $Ti^{3+}_{sub-surf}$.

To clarify the role of HF in the forming of Ti^{3+}, we have investigated the effects of low HF concentration on the synthesis of TiO_2, as shown in Figure S1d and Figure S1e. Compared with P25, when there is no HF addition, there exists Ti^{3+}_{surf} and no F element in R_{F-0}, indicating that the forming of Ti^{3+}_{surf} can be attributed to the solvothermal condition. When the relative ratio of Ti to F increases from 0 to 0.75, there only exists Ti^{3+}_{surf} progressively increasing and no $Ti^{3+}_{sub-surf}$ signal while there only exists physically adsorbed F increasing and no lattice substituted F, indicating that at low HF concentration, F will not replace the O forming $Ti^{3+}_{sub-surf}$ in the lattice.

To identify the effects of F^-, we used other hydracid (HCl and HBr respectively) as the surfactant to replace HF, which were marked as R_{Cl-4} (the relative mole ratio of Cl:Ti is 4) and R_{Br-4} (the relative mole ratio of Br:Ti is 4). The EPR spectra of R_{F-4}, R_{Cl-4} and R_{Br-4} (Figure S1f) show that there is only Ti^{3+}_{surf} and no $Ti^{3+}_{sub-surf}$ observed in R_{Cl-4}, R_{Br-4} while there are both Ti^{3+}_{surf} and $Ti^{3+}_{sub-surf}$ in R_{F-4}. This result shows that it's F^- rather than Cl^- or Br^- that can cause the lattice doping in TiO_2, forming the $Ti^{3+}_{sub-surf}$ at the relative high surfactant concentration. It's proposed that compared with the Ti-Br bond and the Ti-Cl bond, the size of F is similar to O and Ti-F bond is much stronger than the Ti-O bond, which makes F easier to replace the O in the lattice forming the $Ti^{3+}_{sub-surf}$.

The reaction process can be described as the following chemical reaction equations. During the reaction process,

$$Ti(OC_4H_9)_4+4HF \rightleftharpoons 4TiF_4+4C_4H_9OH \quad (3)$$

$$TiF_4 + 2H_2O \rightleftharpoons TiO_2 + 4HF \quad (4)$$

$$3Ti^{4+} + O^{2-} + F^- \rightleftharpoons Ti^{4+} - F^- + Ti^{3+} - V_o - Ti^{3+} + 0.5O_2 \quad (5)$$

From the equation (5), we can see that F^- will react with TiO_2 and Ti^{3+} is forming with the oxygen vacancy (V_o) existing.

According to the La Mer model,[3] the formation process of our TiO_2 nanocrystals can be divided into three stages: decomposition, nucleation and growth, which can be clearly shown in Figure S3. In our reaction process, all the three hydrolysis stages are affected by the HF. At the decomposition regime, TBOT decomposes and small clusters composed of a few atoms starting from monomers form in the solution, which can be affected by both the H^+ and F^-. The F^- can replace the OH^- to be absorbed on the surface of TiO_2（$\equiv Ti-OH + F^- \rightarrow \equiv Ti-F + OH^-$）, and H^+ can slow down the decomposing rate. As the concentration of the reactive monomers increases to reach the supersaturation level, the reaction system enters the nucleation stage. During this period, due to the relatively high concentration of monomers, F^- won't replace the O of TiO_2. When supersaturation is relieved by the formation of nuclei, the system enters the first growth stage, in which no additional nuclei will form but only existing clusters grow larger. As the reaction proceeds and the relative ratio of F^- to TBOT becomes higher and higher, F^- will react with TiO_2 more and more rapidly, triggering the replacement of O and forming the defected shell structure. After the rapid reaction process,

the system enters the second growth stage, and the growth of TiO_2 will be slower and slower until the reaction comes to the balance period, and the Ti^{3+}_{surf} forms on the shell surface of TiO_2.

In conclusion, HF plays an important role in all the three hydrolysis stages and shows different effects as the relative ratio of HF to the monomers changes dynamically, and $Ti^{3+}_{sub-surface}$ and Ti^{3+}_{surf} are forming associated with the relative high ratio of HF to the monomers. Hence, it's a fluorine-assisted dynamic hydrolysis mechanism in the forming process of defective TiO_2. The proposed reaction mechanism can clearly explain the formation process of prepared defective TiO_2 reasonably and the refined structure of prepared defective TiO_2 gives the detailed information about the relationship between Ti^{3+} and the core/shell structure, which can help us control the synthesis of defective TiO_2 with the specific concentration of $Ti^{3+}_{sub-surf}$ and Ti^{3+}_{surf} precisely.

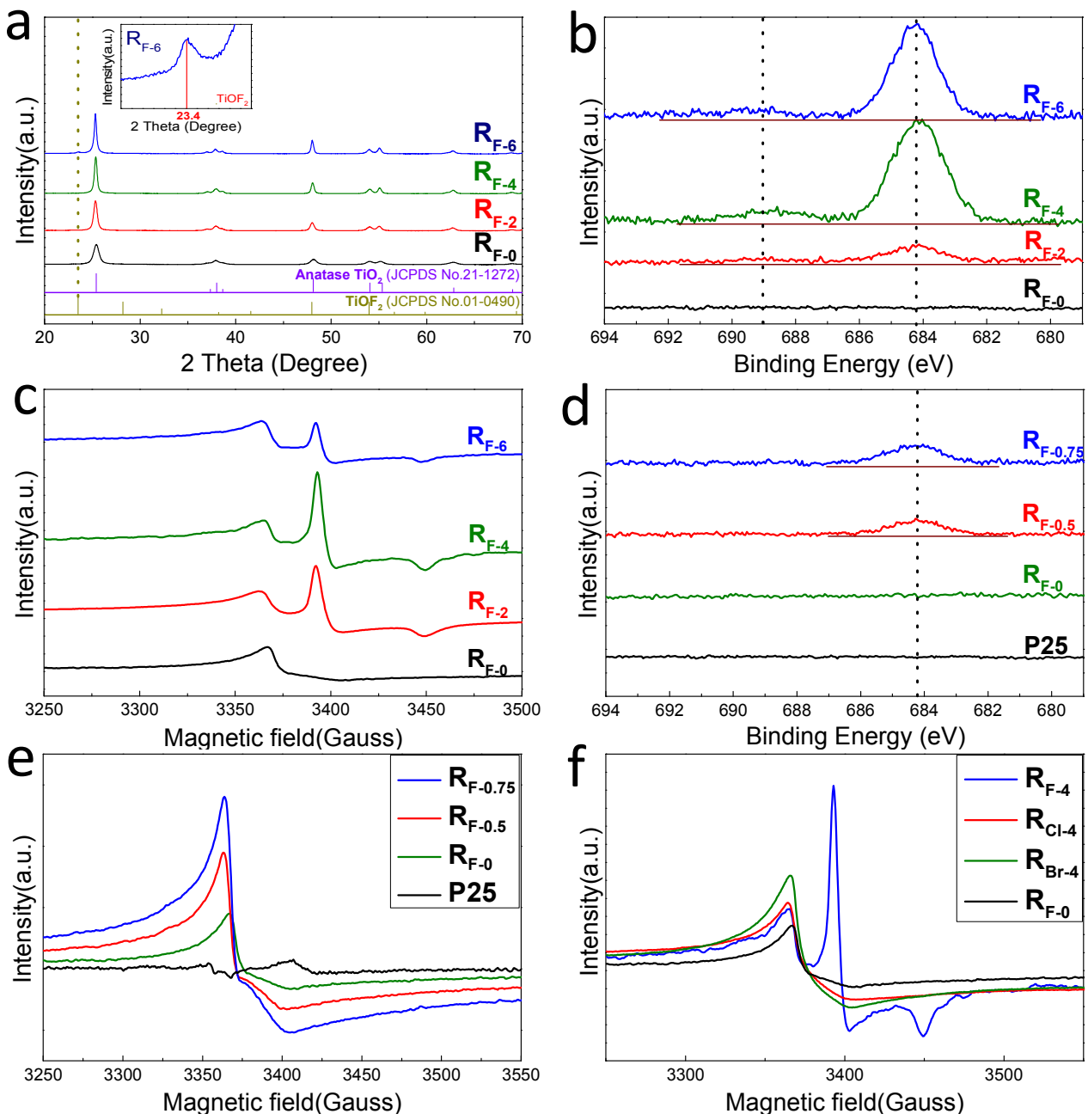

Figure S1. The role of HF in the synthesis of defective TiO_2. (a,b,c) XRD, XPS F1s and EPR spectra of prepared samples R_{F-0}, R_{F-2}, R_{F-4} and R_{F-6}. The inset in (a): the most intense XRD peak of $TiOF_2$ in R_{F-6}. (d,e) XPS F1s and EPR spectra of prepared samples R_{F-0}, $R_{F-0.5}$, $R_{F-0.75}$ and P25. (f) EPR spectra of prepared samples R_{F-0}, R_{F-4}, R_{Cl-4} and R_{Br-4}.

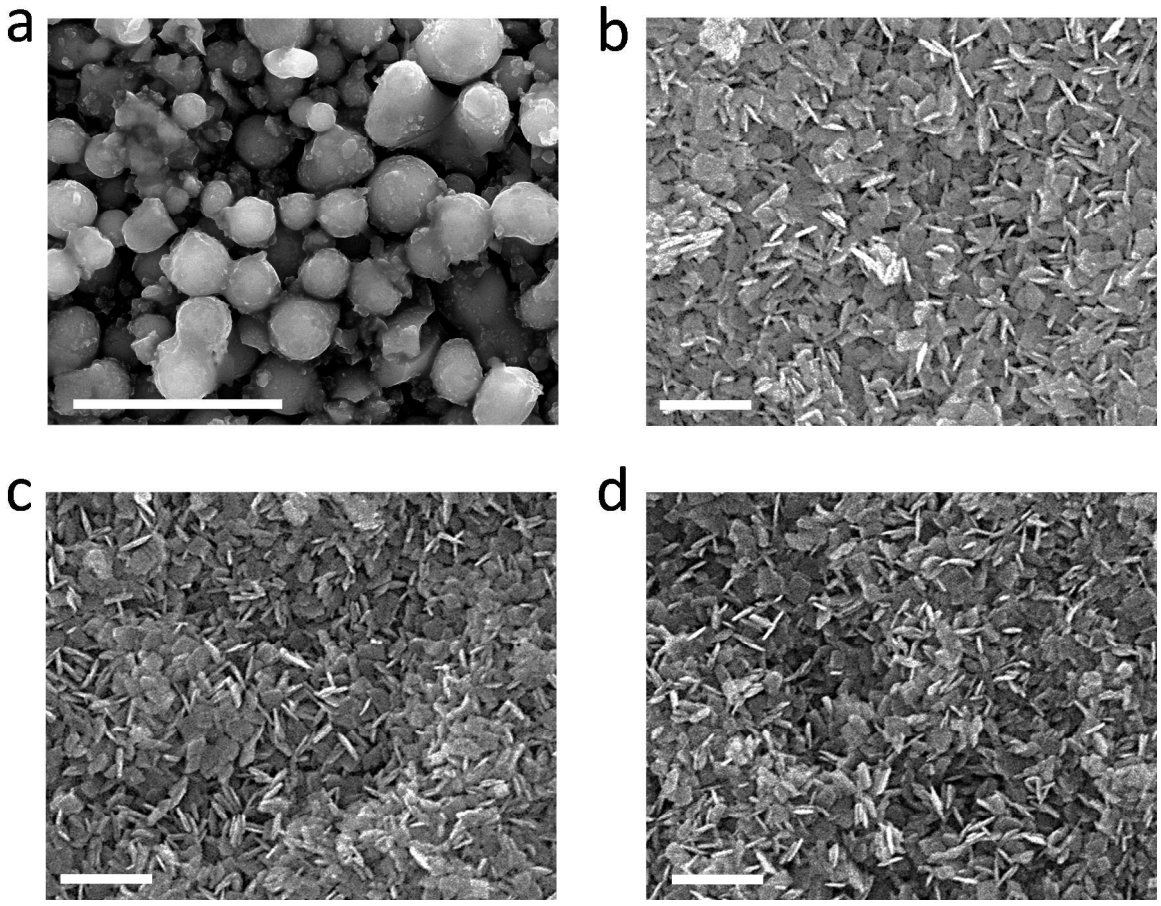

Figure S2. The morphology of defective samples R_{F-0}, R_{F-2}, R_{F-4} and R_{F-6}. (a) SEM image of R_{F-0}. Scale bar: 20 μm. (b~d) SEM images of R_{F-2}, R_{F-4} and R_{F-6}. Scale bar: 100 nm.

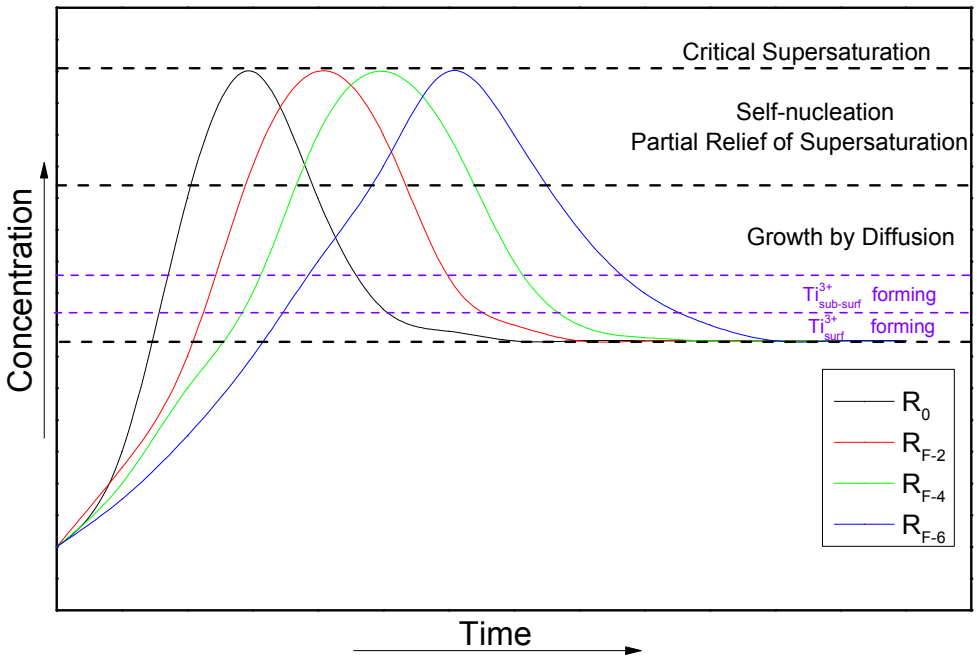

Figure S3. The suggested dynamic hydrolysis mechanism to explain the forming process of defective TiO_2.

2. Detailed characterization of designed TiO_2 and reference samples

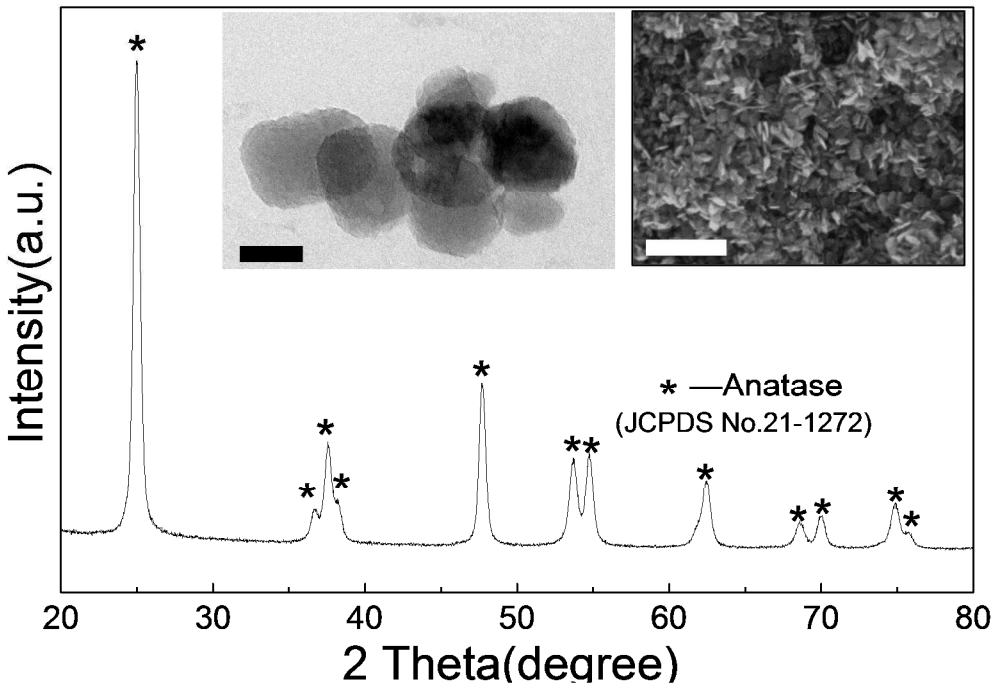

Figure S4. X-ray diffraction spectrum of defective TiO_2(R_{F-4}). Inset: (left) Transmission electron microscopy image of defective TiO_2 (R_{F-4}). The scale bar is 20 nm. (right) Scanning electron microscopy image of prepared defective TiO_2 (scale bar 200 nm).

As shown in Figure S4, the XRD spectrum of defective TiO_2(R_{F-4}) indicates that the prepared TiO_2 is highly crystallized with the anatase phase (JCPDS No.21-1272).

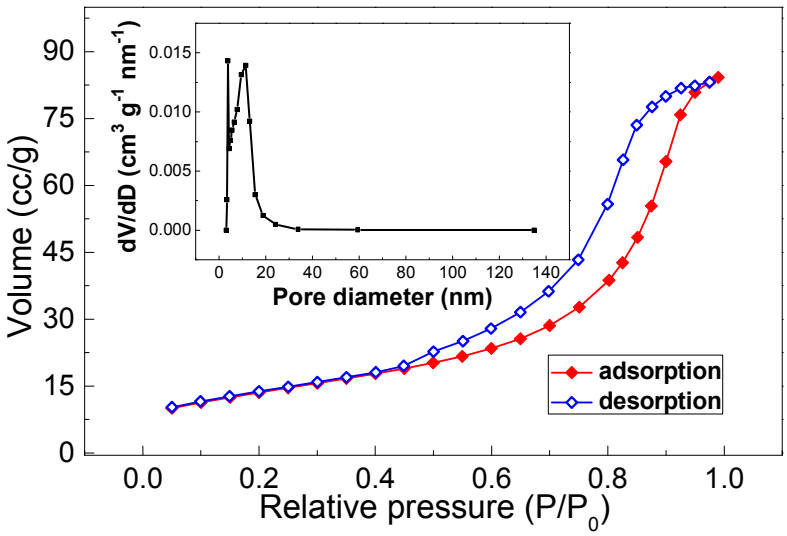

Figure S5. Nitrogen adsorption-desorption isotherms of defective TiO_2 (R_{F-4}). Inset: BJH pore-size distributions of prepared defective TiO_2.

As shown in Figure S5, the pore diameter of defective TiO_2 (R_{F-4}) mostly falls on 10~15 nm. The BET surface area of defective TiO_2 (R_{F-4}) is 49.0 m^2/g similar to that of the commercial Degussa P25 TiO_2 (a mixture of anatase and rutile TiO_2) which is 53.2 m^2/g.

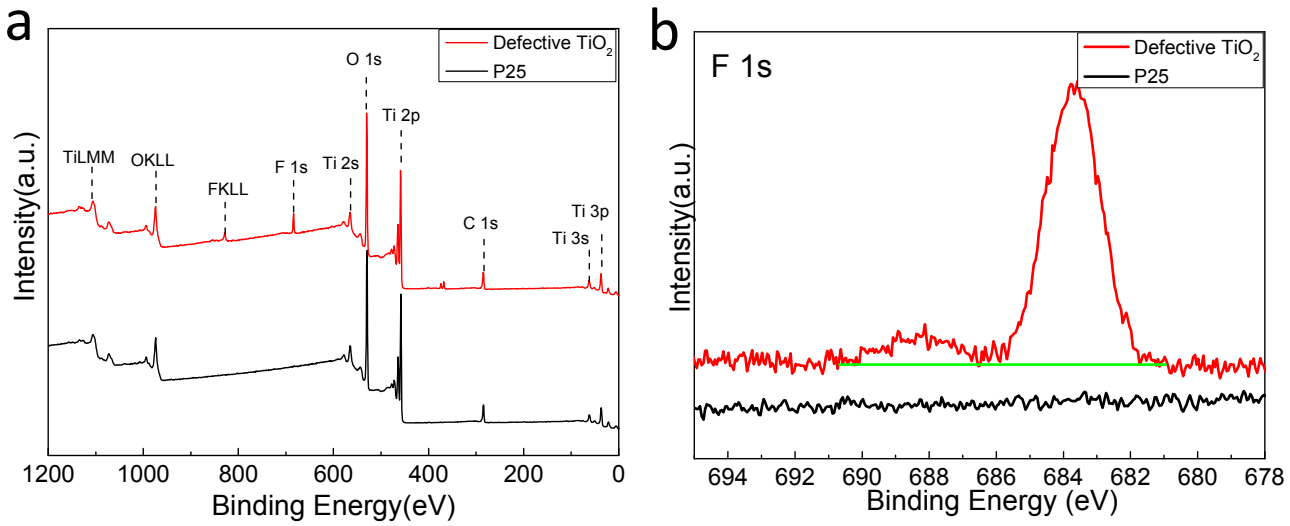

Figure S6. XPS detection of F in defectiveTiO_2 (R_{F-4}). (a) The XPS survey spectra of defective TiO_2 (R_{F-4}) and P25. (b) The high resolution XPS F 1s spectra of defective TiO_2 (R_{F-4}) and P25.

As shwon in Figure S6a, the XPS survey spectrum shows that there exists F element in defective TiO_2 (R_{F-4})and the high resolution XPS spectra of F 1s (Figure S6b) shows there are two peaks. The peak at 684.4 eV is assigned to the F anions that are physically adsorbed on the surface of defectiveTiO_2 (≡Ti-F) while the peak at 689.0 eV denotes the presence of F anions in the crystal lattice.[4-6]

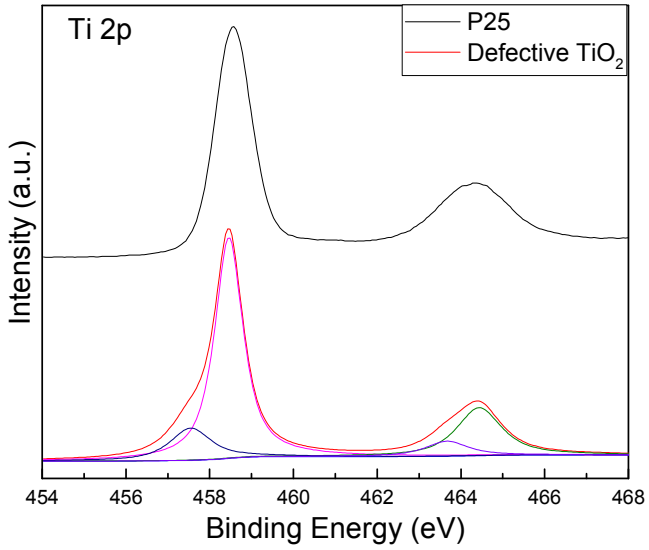

Figure S7. XPS Ti 2p of P25 and defective TiO_2.

For crystalline P25, there are only two only peaks at about 458 nm and 464 nm representing Ti^{4+}, while there are another two peaks at 457.5 nm and 463.7 nm for prepared TiO_2, which indicates that there is Ti^{3+} in the synthesized TiO_2[7-8]. This result corresponds to our EELS and EPR characterization.

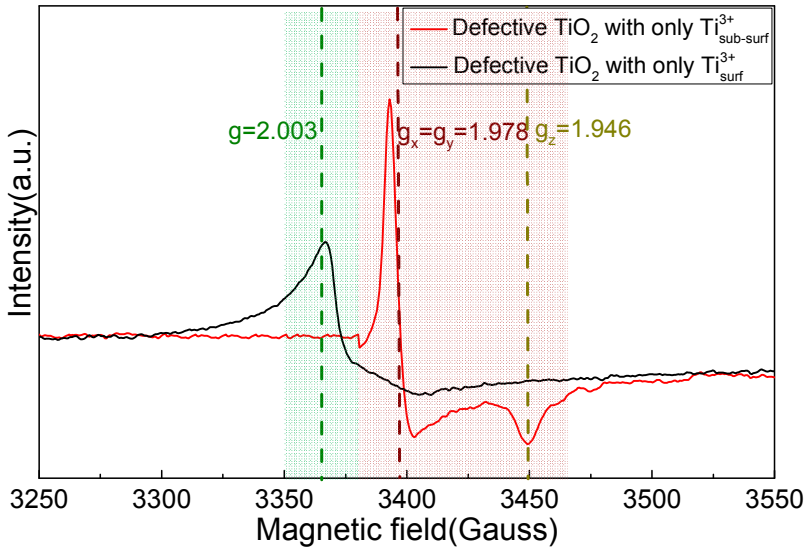

Figure S8. EPR spectra of prepared TiO_2 with only $Ti^{3+}_{sub-surf}$ and TiO_2 with only Ti^{3+}_{surf}

The presence of Ti^{3+} in the prepared samples was investigated by electron paramagnetic resonance (EPR), as shown in Figure S7. The EPR spectra show that only Ti^{3+}_{surf} is existing in HF treated commercial anatase TiO_2 because there is only one signal observed at g=2.003. In addition, only $Ti^{3+}_{sub-surf}$ is existing in air-annealed defective TiO_2 due to the observed anisotropic powder pattern g-values of $g_x=g_y=1.978$ and $g_z=1.946$.

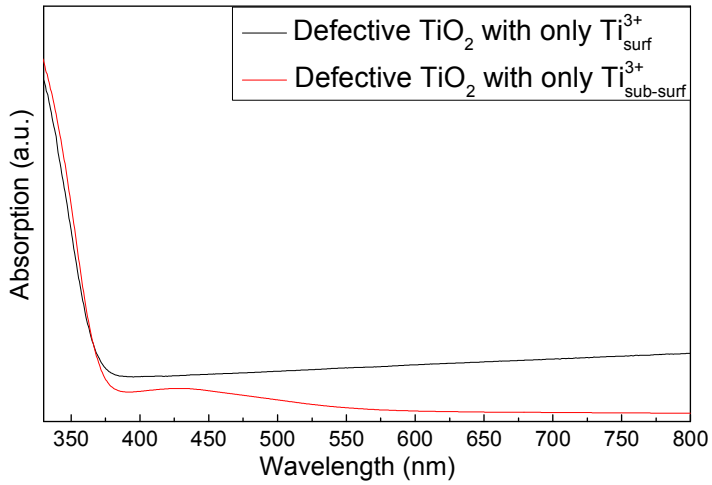

Figure S9. Diffusive reflectance UV−Vis spectra of prepared defective TiO_2 and P25.

The figure S9 shows that TiO_2 with only Ti^{3+}_{surf} and TiO_2 with only $Ti^{3+}_{sub-surf}$ defects can absorb the visible light but their bandgaps are nearly the same about 3.2 eV. Compared with the ~2.6 eV of R_{F-4} with bout Ti^{3+}_{surf} and $Ti^{3+}_{sub-surf}$, it can be indicated that only the co-existence of both Ti^{3+}_{surf} and $Ti^{3+}_{sub-surf}$ can lead to the narrower bandgap.

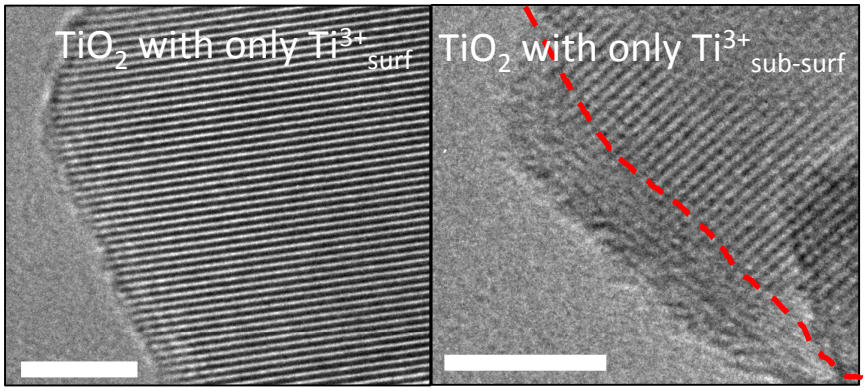

Figure S10. The HRTEM images of TiO_2 with only Ti^{3+}_{surf} and only $Ti^{3+}_{sub\text{-}surf}$. Scale bar: 5 nm.

We have added the HRTEM images of TiO_2 with only Ti^{3+}_{surf} and only $Ti^{3+}_{sub\text{-}surf}$ defects in the revised version, which presented as Figure S10. It shows that there is no obvious disordered layer in TiO_2 with only Ti^{3+}_{surf} while there is ~3 nm disordered layer in TiO_2 with only $Ti^{3+}_{sub\text{-}surf}$. This may be attributed to the synthesis method of TiO_2 with only $Ti^{3+}_{sub\text{-}surf}$. The TiO_2 with only $Ti^{3+}_{sub\text{-}surf}$ is synthesized by annealing the $R_{F\text{-}4}$ under air, so the surface Ti^{3+} can be oxidized while the $Ti^{3+}_{sub\text{-}surf}$ still remains under certain reaction condition.

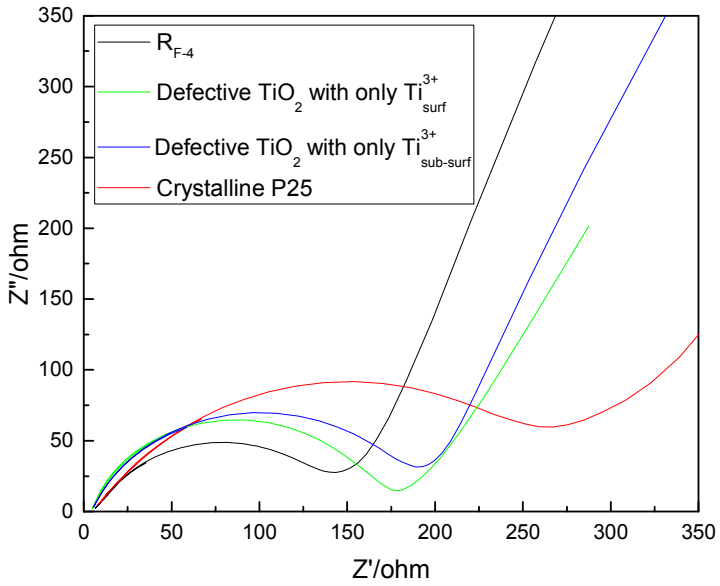

Figure S11. EIS for $R_{F\text{-}4}$, crystalline P25, TiO_2 with only $Ti^{3+}_{sub-surf}$ and TiO_2 with only Ti^{3+}_{surf}

Electrochemical impendance spectra (EIS) for $R_{F\text{-}4}$, crystalline P25, TiO_2 with only $Ti^{3+}_{sub-surf}$ and TiO_2 with only Ti^{3+}_{surf} excluding the effects of light absorbance have been investigated to further clarify the effects on DD tailoring, as shown in SI Fig.8. This EIS result supports that our suggested synergetic charge-carriers transmission mechanism enhancing the carriers transport initiates from the DD tailoring, ruling out the effects of light irradiation.

The working electrodes were fabricated by coating a slurry containing 80 wt% of active materials (P25 and our synthesized samples), 10 wt% of acetylene black (Super-P), and 10 wt% of polyvinylidene fluoride (PVDF) dissolved in N-methyl-2-pyrrolidinone onto a copper foil and dried at 100 °C in vacuum for 12 h before pressing. Standard CR2032-type coin cells were assembled in an Ar-filled glovebox (KIYON, Korea) by using the as-prepared anode, Li metal foil (0.4 mm thick) as the counter electrode, and a separator (Solupor 7P03A). Electrochemical impedance spectra (EIS) were measured using the same electrochemical workstation by applying an AC voltage of 10 mV amplitude over the frequency range from 100 kHz to 0.1 Hz.

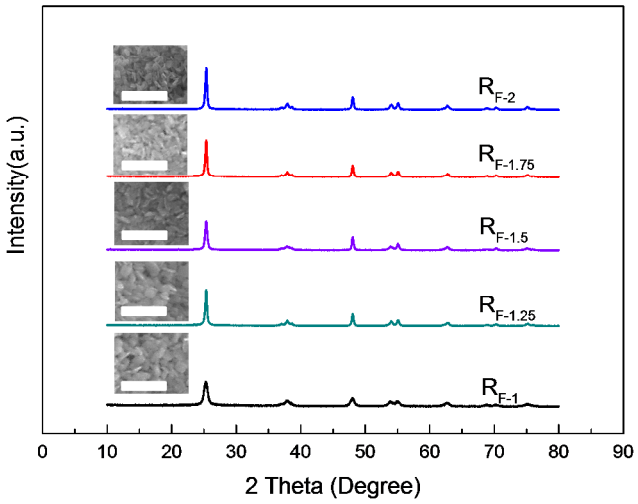

Figure S12. The XRD spectra of R_{F-1}, $R_{F-1.25}$, $R_{F-1.5}$, $R_{F-1.75}$ and R_{F-2}. The insets are the SEM imgaes of prepared TiO_2 (scale bar: 60nm).

As is shown in Figure S9, the XRD spectra and SEM images (the insets in Figure S11) indicate that the samples R_{F-1}, $R_{F-1.25}$, $R_{F-1.5}$, $R_{F-1.75}$ and R_{F-2} have nearly the same morphology and polymorph.

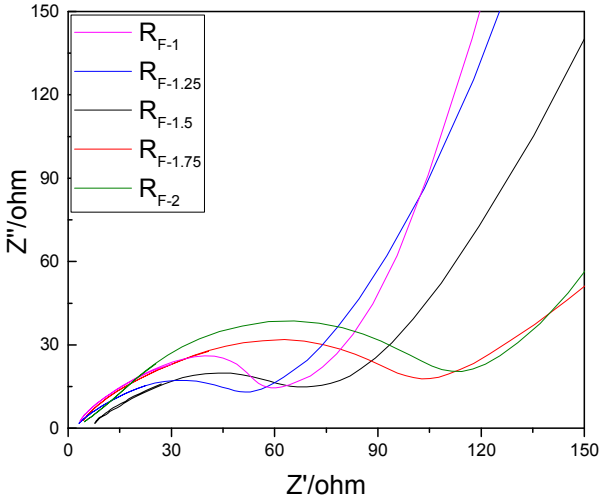

Figure S13. EIS for R_{F-1}, $R_{F-1.25}$, $R_{F-1.5}$, $R_{F-1.75}$, R_{F-2}.

As shown in Figure S10, the EIS shows that all the plots of the samples comprise two semicircles followed by an inclined linear tail. The diameters of the first and second semicircles correspond to the resistances caused by the solid

electrolyte inter-face film (R_f) and the charge transfer resistance (R_{ct}). For the samples R_{F-1}, $R_{F-1.25}$, $R_{F-1.5}$, $R_{F-1.75}$, R_{F-2}, as the RTT decreases from 1.6 (R_{F-2}) to 0.34 ($R_{F-1.25}$), the R_{ct} decreases progressively and the 0.18 (R_{F-1}) shows the worse performance than 0.34 ($R_{F-1.25}$). These results are consistent with our suggested synergetic charge-carriers transmission mechanism. The proper defection distribution can promote the carriers kinetics and the optimal RTT is 0.34.

Table S1. PL lifetimes and fractional intensities of four kinds of TiO_2.

Sample	τ_1/ ns	f_1	τ_2/ ns	f_2	τ_{ave}/ ns
TiO_2 with both surface and sub-surface Ti^{3+}	0.523	0.671	5.282	0.329	2.09
TiO_2 with surface Ti^{3+}	0.505	0.515	5.788	0.485	3.07
TiO_2 with sub-surface Ti^{3+}	0.502	0.494	5.412	0.506	2.99
P25	0.563	0.491	5.869	0.509	3.26

Table S2. Comparison of the photocatalytic hydrogen generation from water splitting of the prepared designed TiO_2 $R_{F-1.25}$ with previously reported anatase TiO_2.

Photocatalyst	Incident light	Photocatalysis parameters	H_2 generation rate (mmol/g/g)	Reference
Hydrogenated anatase TiO_2	AM1.5	0.6 wt.% Pt loading in 1:1 methanol/H_2O	~10	Science. 2011. 331. 746-750[9]
Hydrogenated ordered mesoporous anatase TiO_2	AM.15	1 wt.% Pt loading in 1:4 methanol/H_2O	1.362	J. Am. Chem. Soc. 2014, 136, 9280−9283[10]
Anatase TiO_2 by Al reduction	AM1.5	0.5 wt.% Pt loading in 1:4 methanol/H2O	7.4	Energy Environ. Sci., 2014, 7, 967–972[11]
Hydrogenated anatase TiO_2	AM1.5	0.5 wt.% Pt loading in 1:4 methanol/H_2O	8.2	Adv. Funct. Mater., 2013, 23, 5444[12]
Hydrogenated anatase TiO_2	AM 1.5	1.0 wt. % Pt loading in 1:4 CH_3OH/H_2O	2.15	Chem. Commun. 2012, 48, 5733-5735[13]
P25			0.57	

S doped H-TiO_2	AM 1.5	0.5 wt. % Pt loading in 1:3 CH_3OH/H_2O	0.258	J. Am. Chem. Soc. 2013, 135, 17831-17838[14]
Defective anatase TiO_2 ($R_{F-1.25}$)	AM 1.5	1 wt. % Pt loading in 1:4 CH_3OH/H_2O	13.21	Our work
P25			0.54	

3. References

(1) Wang, Z. Y.; Lv, K. L.; Wang, G. H.; Deng, K. J.; Tang, D. G. Study on the Shape Control and Photocatalytic Activity of High-energy Anatase Titania. *Appl. Catal. B-environ* **2010,** *100*, 378-385.

(2) Zuo, F.; Wang, L.; Wu, T.; Zhang, Z. Y.; Borchardt, D.; Feng, P. Y. Self-Doped Ti^{3+} Enhanced Photocatalyst for Hydrogen Production under Visible Light. *J. Am. Chem. Soc.* **2010,** *132*, 11856-11857.

(3) Cargnello, M.; Gordon, T. R.; Murray, C. B. Solution-phase Synthesis of Titanium Dioxide Nanoparticles and Nanocrystals. *Chem. Rev.* **2014,** *114*, 9319-9345.

(4) Naldoni, A.; Allieta, M.; Santangelo, S.; Marelli, M.; Fabbri, F.; Cappelli, S.; Bianchi, C. L.; Psaro, R.; Dal Santo, V. Effect of Nature and Location of Defects on Bandgap Narrowing in Black TiO_2 Nanoparticles. *J. Am. Chem. Soc.* **2012,** *134*, 7600-7603.

(5) Czoska, A.; Livraghi, S.; Chiesa, M.; Giamello, E.; Agnoli, S.; Granozzi, G.; Finazzi, E.; Valentin, C. D.; Pacchioni, G. The Nature of Defects in Fluorine-doped TiO_2. *J. Phys. Chem. C* **2008,** *112*, 8951-8956.

(6) Gordon, T. R.; Cargnello, M.; Paik, T.; Mangolini, F.; Weber, R. T.; Fornasiero, P.; Murray, C. B. Nonaqueous Synthesis of TiO_2 Nanocrystals using TiF_4 to Engineer Morphology, Ooxygen Vacancy Concentration, and Photocatalytic Activity. *J. Am. Chem. Soc.* **2012,** *134*, 6751-6761.

(7) Chen, J.; Song, W.; Hou, H.; Zhang, Y.; Jing, M.; Jia, X.; Ji, X. Ti^{3+} Self-Doped Dark Rutile TiO_2 Ultrafine Nanorods with Durable High-Rate Capability for Lithium-Ion Batteries. *Adv. Funct. Mater.* **2015,** *25*, 6793-6801.

(8) Cui, H.; Zhao, W.; Yang, C.; Yin, H.; Lin, T.; Shan, Y.; Xie, Y.; Gu, H.; Huang, F. Black TiO_2 Nanotube Arrays for High-efficiency Photoelectrochemical Water-splitting. *J. Mater. Chem. A* **2014,** *2*, 8612-8616.

(9) Chen, X.; Liu, L.; Yu, P. Y.; Mao, S. S. Increasing Solar Absorption for Photocatalysis with Black Hydrogenated Titanium Dioxide Nanocrystals. *Science* **2011,** *331*, 746-750.

(10) Zhou, W.; Li, W.; Wang, J. Q.; Qu, Y.; Yang, Y.; Xie, Y.; Zhang, K.; Wang, L.; Fu, H.; Zhao, D. Ordered Mesoporous Black TiO_2 as Highly Efficient Hydrogen Evolution Photocatalyst. *J. Am. Chem. Soc.* **2014,** *136*, 9280-9283.

(11) Lin, T.; Yang, C.; Wang, Z.; Yin, H.; Lu, X.; Huang, F.; Lin, J.; Xie, X.; Jiang, M. Effective Nonmetal Incorporation in Black Titania with Enhanced Solar Energy Utilization. *Energy Environ. Sci.* **2014,** *7*, 967-972.

(12) Wang, Z.; Yang, C.; Lin, T.; Yin, H.; Chen, P.; Wan, D.; Xu, F.; Huang, F.; Lin, J.; Xie, X.; Jiang, M. H-Doped Black Titania with Very High Solar Absorption and Excellent Photocatalysis Enhanced by Localized Surface Plasmon Resonance. *Adv. Funct. Mater.* **2013,** *23*, 5444-5450.

(13) Zheng, Z.; Huang, B.; Lu, J.; Wang, Z.; Qin, X.; Zhang, X.; Dai, Y.; Whangbo, M.-H. Hydrogenated Titania: Synergy of Surface Modification and Morphology Improvement for Enhanced Photocatalytic Activity. *Chem. Commun.* **2012,** *48*, 5733-5735.

(14) Yang, C.; Wang, Z.; Lin, T.; Yin, H.; Lü, X.; Wan, D.; Xu, T.; Zheng, C.; Lin, J.; Huang, F.; Xie, X.; Jiang, M. Core-shell Nanostructured "Black" Rutile Titania as Excellent Catalyst for Hydrogen Production Enhanced by Sulfur Doping. *J. Am. Chem. Soc.* **2013,** *135*, 17831-17838.